Aldehyde Hydrogenation by Pt/TiO$_2$ Catalyst in Aqueous Phase: Synergistic Effect of Oxygen Vacancy and Solvent Water

Wei Cao, Guang-Jie Xia,* Zhen Yao, Ke-Han Zeng, Ying Qiao, and Yang-Gang Wang*

Read Online

ACCESS | Metrics & More | Article Recommendations | Supporting Information

ABSTRACT: The aldehyde hydrogenation for stabilizing and upgrading biomass is typically performed in aqueous phase with supported metal catalysts. By combining density functional theory calculations and ab initio molecular dynamics simulations, the model reaction of formaldehyde hydrogenation with a Pt/TiO$_2$ catalyst is investigated with explicit solvent water molecules. In aqueous phase, both the O vacancy (Ov) on support and solvent molecules could donate charges to a Pt cluster, where the Ov could dominantly reduce the Pt cluster from positive to negative. During the formaldehyde hydrogenation, the water molecules could spontaneously protonate the O in the aldehyde group by acid/base exchange, generating the OH* at the metal−support interface by long-range proton transfer. By comparing the stoichiometric and reduced TiO$_2$ support, it is found that the further hydrogenation of OH* is hard on the positively charged Pt cluster over stoichiometric TiO$_2$. However, with the presence of Ov on reduced support, the OH* hydrogenation could become not only exergonic but also kinetically more facile, which prohibits the catalyst from poisoning. This mechanism suggests that both the proton transfer from solvent water molecules and the easier OH* hydrogenation from Ov could synergistically promote aldehyde hydrogenation. That means, even for such simple hydrogenation in water, the catalytic mechanism could explicitly relate to all of the metal cluster, oxide support, and solvent waters. Considering the ubiquitous Ov defects in reducible oxide supports and the common aqueous environment, this synergistic effect may not be exclusive to Pt/TiO$_2$, which can be crucial for supported metal catalysts in biomass conversion.
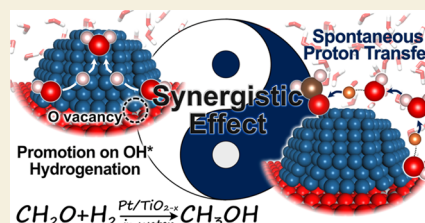
KEYWORDS: aqueous phase, reducible oxide support, aldehyde hydrogenation, supported metal catalyst, Pt/TiO$_2$

INTRODUCTION

Using nonedible biomass to replace traditional petrochemical feedstocks is a promising strategy to reduce carbon emissions, which has become a new trend in developing green catalysis.[1,2] After the primary fast pyrolysis or liquefaction, the biomass feeds generally contain oxygenates including carboxylic acids, aldehydes, ketones, alcohols, ethers, and phenolic compounds.[3−5] Compared to the conventional high-energy fuels, these biomass feeds are oxygen-rich and hydrogen-poor with relatively low calorific values. More importantly, the phenolic condensation and the self-aldol condensation of aldehydes could make the biomass a mass coke.[6,7] Therefore, to increase both the energy density and stability, further upgrading of the biomass feeds by hydrodeoxygenation (HDO) reactions is necessary.[8−11] Among them, the hydrogenation of aldehyde groups could be one of the most important procedures.[12,13] For example, furfural as a promising platform compound can be converted to furfuryl alcohol through aldehyde group hydrogenation in industries.[14] Besides, the selective hydrogenation of α,β-unsaturated aldehydes to their corresponding unsaturated alcohols is also the key reaction to produce fragrances and agrochemicals.[15]

The supported metal catalysts have been extensively applied to aldehyde hydrogenations due to their excellent performance and adjustable surface properties.[16,17] The metal clusters or nanoparticles are usually supported on oxide supports with a high surface area and strong stability, such as TiO$_2$, CeO$_2$, ZrO$_2$, SiO$_2$, Al$_2$O$_3$, etc.[17] Besides the decisive influence of metal, in many cases, the oxide supports can largely determine the catalytic activity of hydrogenation.[18] It has been widely accepted that reducible oxide support, especially TiO$_2$, could promote catalytic hydrogenation.[19−21] This intrinsic mechanism could be highly attributed to the ubiquitous oxygen vacancies (Ov) (or effectively the interstitial Ti defect) within the reduced support.[22−25] On the one hand, the Ov could participate as the active sites in the catalytic reaction, especially for reactant and intermediate adsorptions. For example, the isotopic experiment by Kalamaras et al. unveiled that the Ov formation is directly involved in the water gas shift reaction by Pt/TiO$_2$.[26] On the other hand, the presence of Ov could enhance the hydrogenation selectivity. For instance, the Ov can anchor and activate the aldehyde group of crotonaldehyde by forming a crotyl-oxy surface intermediate, resulting in a

more favorable selectivity for crotyl alcohol.[19] Moreover, the Ov sites could induce the charge transfer from the reduced TiO_2 surface to the metal cluster, which leads to negatively charged metal clusters with higher activity for reactions like CO oxidation[24] and oxygen reduction.[27] This active charge transfer also makes the Ov sites on the TiO_{2-x} surface become the growth center for Pt nanoparticles and assist to activate Pt species.[28,29]

Almost all of the abovementioned studies on how Ov influences the catalytic performance are done in the gas phase. Meanwhile, due to the low volatility and the hard separation of the oxygen-containing chemicals, catalytic reactions of biomass often occur at the solid/liquid interface in various solutions, especially in water.[30,31] It has been known that water molecules could play critical roles in catalytic reactions. For example, the solvent water could slightly change the electronic properties of the supported metal cluster,[32] modify the solvent–shell-mediated dynamics,[33] facilitate the catalytic proton transfer steps,[34] and stabilize the intermediates with hydrogen bonds.[33,35−37] However, when it comes to the aldehyde hydrogenation by M/TiO_{2-x} in aqueous phase, how the solvent water mechanically influences the catalytic cycle is still unclear. In addition, could the Ov have a decisive impact on the metal catalysts in aqueous phase like that in gas phase? Is there any synergistic effect between Ov sites and solvent water molecules? Considering the hard experimental characterization in aqueous phase,[38,39] a dynamic theoretical simulation of catalytic aldehyde hydrogenation could be quite helpful for answering these questions.

The main difficulty of this simulation in aqueous phase comes from the well-known dynamic property of solvent molecules.[34,37,40−42] This effect can be critical for aldehyde hydrogenation in aqueous phase, where the protonation of carbonyl via the hydrogen exchange[34,43] and the following long-range proton transfer[44,45] can take place. Hence, the abundant explicit solvent molecules are essential for the realistic modeling of this catalytic system.[46] Although there are few theoretical investigations on biomass hydrogenation with the implicit solvation model[47] or involving several explicit adjacent solvent waters,[48] there is still no theoretical study of aldehyde hydrogenation in aqueous phase within the more realistic ternary model,[49] involving all of the metal cluster, oxide support, and explicit solvent waters. As the more complex aldehydes call for the larger metal cluster for adsorption and in turn the larger TiO_2 support surface, here, the hydrogenation of the simplest aldehyde, formaldehyde (CH_2O), is investigated as the model reaction of aldehyde hydrogenation for biomass.

In this work, by combining ab initio molecular dynamic (AIMD) simulations and density functional theory (DFT) calculations, we explored the mechanistic insights into the CH_2O hydrogenation in aqueous phase by the more realistic ternary model consisting all of the platinum cluster, the titania support, and the abundant explicit solvent waters. By comparing the mechanisms and free energy barriers of the Pt catalysts over the stoichiometric TiO_2 and reduced TiO_{2-x} support, the synergistic effect between the oxygen vacancy and solvent water molecules is revealed. The solvent water would conduct the long-range proton transfer to assist the O protonation in the aldehyde group and correspondingly generate the OH* at the metal−support interface, whilst the Ov can promote the OH* hydrogenation to prevent catalyst poisoning. This synergistic effect mechanistically confirms the

importance of both the solvent water molecules and oxygen vacancy on reducible oxide support for aldehyde hydrogenation in aqueous phase. That means the catalytic reaction in aqueous phase is not only related to the surface of the metal cluster or nanoparticle. For such a simple hydrogenation reaction, the catalytic mechanism could relate to all of the metal, the oxide support, and the solvent.

■ METHODS

All DFT calculations involving ab initio molecular dynamics (AIMD) simulations and biased AIMD simulations are performed using the CP2K package.[50] The Gaussian and auxiliary plane wave (GPW) double zeta basis set is used to describe the valence electron with the cutoff of 400 Ry, where the Goedecker−Teter−Hutter (GTH)-type pseudopotential is applied to describe the effect of core electrons. The exchange and correlation interactions of valence electrons are calculated by the PBE functional,[51] and the dispersion interaction is presented by Grimme's D3 corrections.[52] The DFT + U method with the effective Hubbard term ($U_{eff} = U − J$) of 4.2 eV is used to describe Ti 3d electrons, which agrees with the values of 4.0−5.0 eV in previous studies.[53,54] With the energy converged to $10^{−6}$ Ry in each self-consistent field (SCF) iteration step, the convergence criterion for the maximum force is 0.02 eV/Å in geometry optimization. The ab initio molecular dynamics (AIMD) simulations are performed to get the equilibrium configuration of catalysts in aqueous phase, while the metadynamics[55,56] (MTD) simulations are used to get the free energy change and barrier of each elementary step. Both the AIMD and MTD simulations undergo within the canonical (NVT) ensemble by Nosé−Hoover thermostats.[57] In AIMD, the temperature is controlled at the typical supporting temperature of 350 K,[58] while in MTD, at the typical reaction temperature of 300 K.[59,60] The last configurations in AIMD simulations will undergo annealing simulations, where the factor for rescaling of speed distribution is 0.998, which is a relatively smoother annealing speed compared to that in previous works.[61,62] The deuterium mass is adopted for all H atoms to get the longer timestep of 1 fs. The AIMD simulations are performed for 15 ps. The equilibrium of AIMD simulations is identified by the potential energy evolution in Figure S2 and the atomic velocity distribution in Figure S3. In MTD, we use the atomic distance as the collective variable (CV), where the detailed parameters are illustrated in Table S5. The reconstruction of free energy surface (FES) as a function of CV is done by summation of the repulsive time-dependent Gaussian-shaped potential added during the MTD simulation.[56,63] The free energy surfaces of elementary steps from MTD simulations are summarized in Figure S11. To avoid possible bias arising from the selection of CV,[56] MTD tests with different kinds of CV are conducted and shown in Figure S12. Further tests on the height of the Gaussian-shaped potential are shown in Figure S13, and those on different starting configurations are shown in Figure S14. Following the reports from Gervasio et al.[64] and Bucko,[65] the MTD simulations stop after the first-time complete access of both the reactant and the product states, where the details are in the Supporting Information.

In the model, the TiO_2 substrate consists of a rutile $TiO_2(110)$ (3 × 3) supercell slab with four O−Ti−O trilayers, where the bottom two trilayers are fixed by constraining the coordinates to their original positions during the simulations. Under the periodic condition, the slab is separated by a vacuum thickness of 20 Å along the Z-direction, which is then filled with 102 water molecules corresponding to the density of around 1.0 g/mL. The model involving a Pt_{14} cluster on the stoichiometric TiO_2 surface is denoted Pt/TiO_2 in Figure S1a. In previous works, the sizes of reported Pt clusters roughly range from 0.5 to 3 nm,[66−68] and even smaller Pt_n clusters ($n < 10$) can be synthesized.[69] Hence, with the size of around 0.7 nm, the Pt_{14} cluster could be proper to theoretically simulate the catalytic reaction of Pt/TiO_2 in aqueous phase. For the reduced TiO_2 surface, an oxygen vacancy (Ov) is formed by removing one bridge oxygen (O_{br}), which corresponds to ∼10% surface O_{br} atoms and is close to the amount of several percent in experiments.[70,71] Previous studies have already shown that the metal clusters will favorably bind on the Ov site,[29,72]
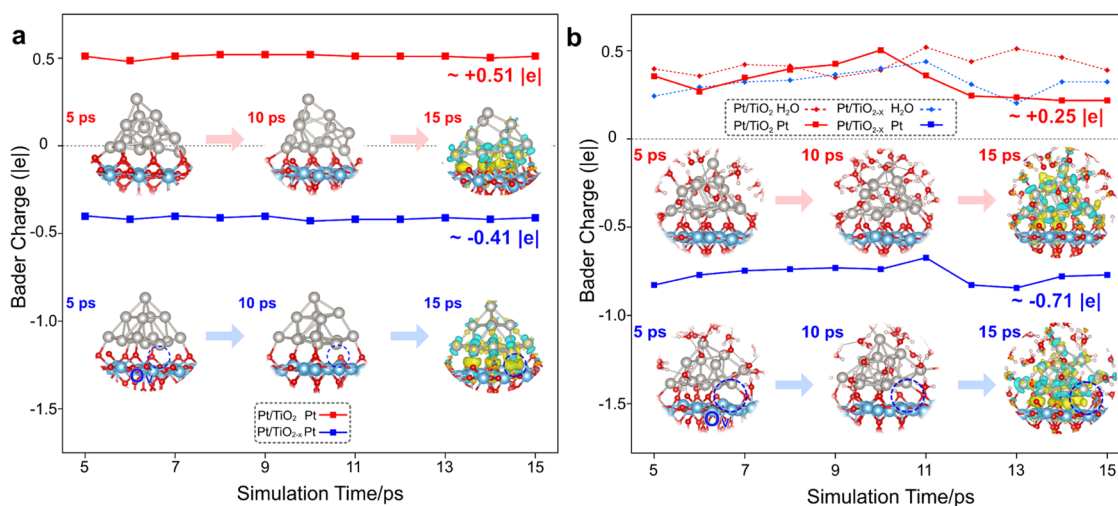
Figure 1. Bader charge of the Pt cluster and representative configurations of the catalyst along with the AIMD simulations in gas phase and aqueous phase. The Pt/TiO$_2$ and Pt/TiO$_{2-x}$ catalysts are represented in red and blue, respectively. (a) Simulation in gas phase. (b) Simulation in aqueous phase. The configurations of the 15 ps show the charge difference between the metal cluster and the remaining system. The electron depletion/accumulation is depicted by blue/yellow isosurfaces at ±0.06 |e| Å^{-3}. The blue dotted circle highlights the localized electron around Ov.

so the pyramid-like Pt$_{14}$ cluster is initially placed over Ov, which model is denoted Pt/TiO$_{2-x}$ in Figure S1b. In some experiments, with H$_2$ pretreatment at the relatively high temperature, some Pt clusters could be fully encapsuled by thin TiO$_{2-x}$ layers, leading to the strong metal−support interaction (SMSI).[73−75] Yet, due to the easy hydrolysis of surface Ov,[76,77] this encapsulation is hard to take place in aqueous phase at the mild temperature, which is not taken into account in the simulations, and the details are discussed in the Supporting Information. For charge analysis, the Bader charges are calculated from the code[78,79] by Henkelman et al. based on the density file of valence electrons.

RESULTS AND DISCUSSION

AIMD Simulations of Pt/TiO$_2$ and Pt/TiO$_{2-x}$ Catalysts

First of all, several ab initio molecular dynamics (AIMD) simulations are performed to compare how the Pt clusters evolve over the stoichiometric TiO$_2$ and reduced TiO$_{2-x}$ support in both gas phase as a reference and aqueous phase. To get the representative configurations of Pt cluster catalysts, the Pt$_{14}$ cluster will undergo the initial geometry optimization on supports, followed by the AIMD simulations of 15 ps at the typical supporting temperature of 350 K[58] for equilibrium. After the annealing processes of 3 ps for cooling to 20 K, the catalysts would be optimized again to get their representative configurations, where the whole process is shown in detail in Figure S1. In both gas and aqueous phases, due to the intrinsic stability and adequate metal−support interaction, the pyramid-like Pt$_{14}$ cluster will not have a big morphology change during all of these AIMD simulations shown in Figure 1. Meanwhile, as reported in previous studies,[71,80] on the reduced oxide support, the Ov could strengthen the metal−support interaction (MSI) by charge transfer. Multiple configurations taken from the trajectories of AIMD simulations are used to get the average binding energies of Pt clusters. As shown in Table S1 and Figure S4, the presence of Ov could lead to the stronger Pt binding by around 1.90 eV in gas phase and around 2.17 eV in aqueous phase. This confirms the anchoring effect of the Ov site on metal clusters observed in previous experiments.[28] These stronger MSI from Ov could be deeply rooted in its decisive influence on charge states of the metal cluster. To identify that, the snapshots of 1 ps interval in the

last 10 ps of AIMD simulations have been collected for the optimizations, followed by charge analyses shown in Figure 1.

Our previous studies[21,24,60] on Au/TiO$_{2-x}$ in gas phase have demonstrated that the Au cluster, which works as the electron reservoir, could show qualitatively distinct charge characteristics over the stoichiometric and reduced TiO$_2$ surface. On the stoichiometry TiO$_2$ surface, the electrostatic (Hartree) potential (V_H)[81] could exist at a relatively high level, making the electron transfer from metal to support, but on the reduced TiO$_{2-x}$ surface, the lower V_H could lead to the reverse electron transfer from support to metal. This trend also stands in the case of Pt and is directly observed recently by the ultrahigh sensitivity and precision electron holography.[82] As shown in Figure 1a, the total Bader charge of the Pt cluster is positive on stoichiometry TiO$_2$ with the charge values around +0.51|e|, while with the extra electrons donated from the Ov site, like Au, the Pt cluster can also act as the electron reservoir on the reduced TiO$_{2-x}$ surface. By receiving electrons, it will conspicuously convert into a negative species around −0.41|el. This suggests that the Ov could dramatically reduce the Pt cluster in gas phase, which well accords with the XPS in experiment.[27]

When it comes to the aqueous phase, the Pt cluster will work as the electron reservoir for not only the Ov but also the solvent water. The added ambient solvent, which includes the water molecules in the liquid phase and adsorbed water molecules on the Pt cluster and support, will integrally take the positive charge around +0.37|e| on Pt/TiO$_2$ and +0.25|e| on Pt/TiO$_{2-x}$. These charges in the solvent water mainly come from the interaction with the Pt cluster. From the gas phase in Figure 1a to the aqueous phase in Figure 1b, the charge of the Pt cluster on TiO$_2$ averagely decreases by 0.26|e|, and that on TiO$_{2-x}$ decreases by 0.30|e|. Those values can mostly cover the positive charges in ambient water molecules. By the more detailed charge analyses shown in Figure S5, it is clear that the electron transfer from solvent waters to Pt cluster mainly comes from the Pt−OH$_2$ bond of these adsorbed water molecules. Yet, the binding between these water molecules and the Pt cluster is quite weak, so they will dynamically underdo the adsorption and desorption processes. These dynamic
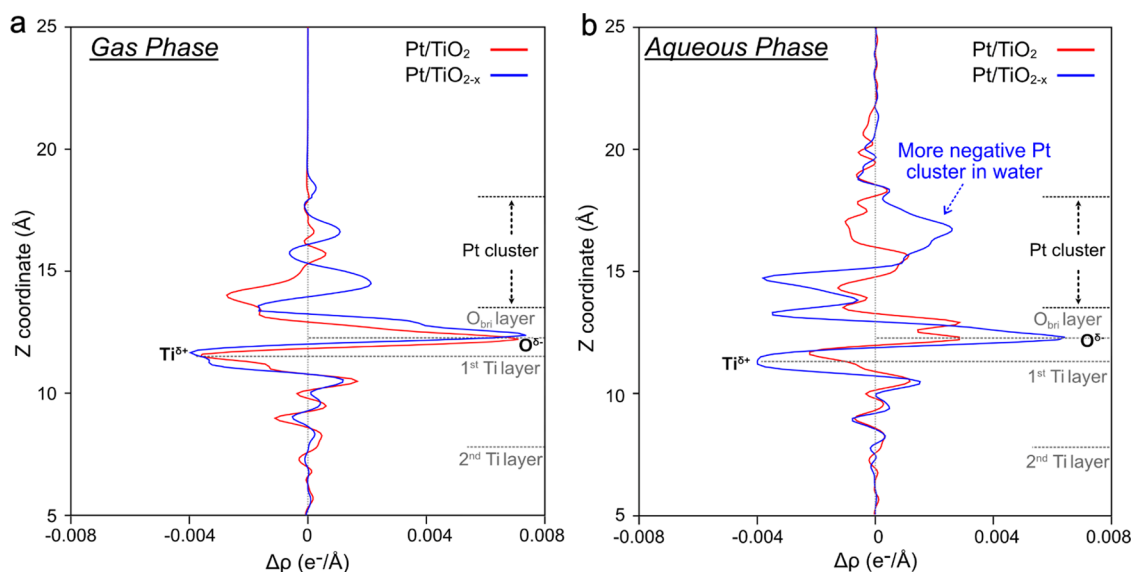
Figure 2. Charge difference integrated in planes perpendicular to the surface ($\Delta\rho(z)$) as a function of the height (z). The positive value of $\Delta\rho$ indicates the accumulation of electrons, while negative $\Delta\rho$ indicates the depletion of electrons. The y-axis label accords with the height of the model as shown in the right notes. (a) Charge difference in gas phase, $\Delta\rho = \rho_{M/S} - \rho_M - \rho_S$. (b) Charge difference in aqueous phase, $\Delta\rho = \rho_{M/S/Aq} - \rho_M - \rho_{S/Aq}$.
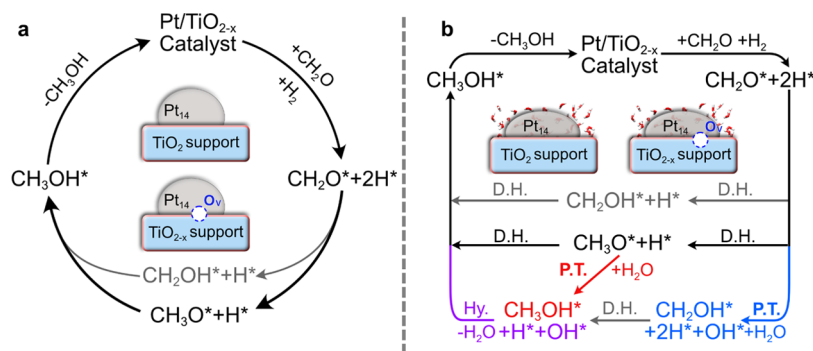

Figure 3. Possible catalytic cycles of CH_2O hydrogenation. (a) Cycle in gas phase. The CH_2OH pathway is colored in gray, while the CH_3O pathway in black. (b) Cycle in aqueous phase. The direct hydrogenation (D.H.) steps have the same colors as those in gas phase. For the steps involving proton transfer (P.T.) in aqueous phase, the CH_2O elementary step is colored in blue, while the CH_3O elementary step is in red.

adsorptions could vary the integral charge of ambient water molecules, which in turn leads to the more fluctuating Pt charge in aqueous phase compared to that in gas phase. Comparatively speaking, the Ov still has a decisive effect on electron donation in aqueous phase, which converts the charge of the Pt cluster qualitatively from positive to negative. The solvent water molecules also provide electrons to the Pt cluster by dynamic water adsorptions, but this plays a relatively minor role.

To further investigate the effects of Ov and solvent water molecules, we calculated the charge difference between the metal and the remaining system, where its planar average along the Z-direction is plotted in Figure 2.

In gas phase, the adsorption of the Pt cluster would lead to the obvious polarization of the surface TiO_2 layer. With the formation of $Pt-O_{br}$ bonds, the protuberant O_{br} atoms will receive some electrons, while the planar Ti layer including the Ti and $O_{(3c)}$ atoms will lose some electrons. On the stoichiometric TiO_2 surface, the electrons will generally transfer from the metal cluster to TiO_2 support, leading to the oxidation of the cluster and partial reduction of the support. Because of this transfer, the bottom of the pyramid-

like Pt_{14} cluster will be positively charged. When one introduces the O vacancy on the TiO_2 surface, the polarization of the surface TiO_{2-x} layer (blue line) is similar to that without Ov (red line) in Figure 2a. This means the similar electron accumulation on the protuberant O_{br} atoms from the $Pt-O_{br}$ bonds. Meanwhile, by reducing the TiO_2 surface by one Ov, the introduced two electrons will make the net charge transfer from the reduced TiO_{2-x} support to the metal. The reduced support will be partially oxidized, while the Pt cluster will be reduced to be negatively charged.

In aqueous phase, the charge transfer direction is basically the same. Besides the slight charge transfer from ambient water molecules to the Pt cluster, the explicit water molecules will also influence the polarization of the surface TiO_2 layer. On the stoichiometric TiO_2 surface, the charge exchange between the Pt and surface O_{br} atoms in aqueous phase is less obvious than that in gas phase. This is probably because of the active interaction between the positive Pt cluster and the negative OH groups ($HO_{top}-Ti$) coming from surface hydration ($H_2O_{top}-Ti + O_{br} \rightarrow HO_{top}-Ti + O_{br}H$). As shown in Figure S6, in AIMD simulations, we can even observe the occasional OH exchange between the support and Pt cluster at their
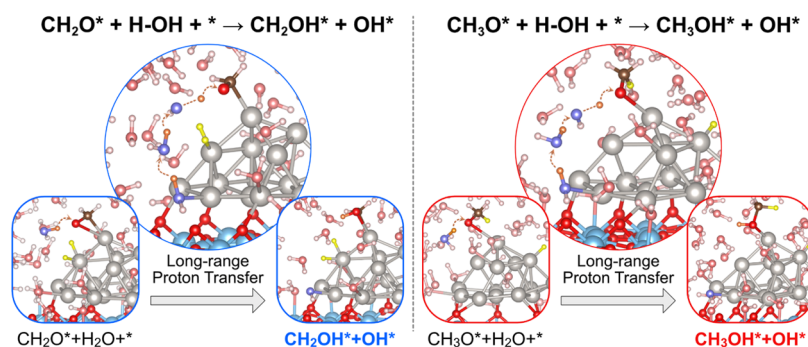
Figure 4. Typical configurations during the two spontaneous long-range proton transfer processes over Pt/TiO_{2-x}. The configurations in the same processes over Pt/TiO_2 are similar. These P.T. steps could be observed in AIMD simulations, while all of the G_a and ΔG values are obtained by MTD simulations.
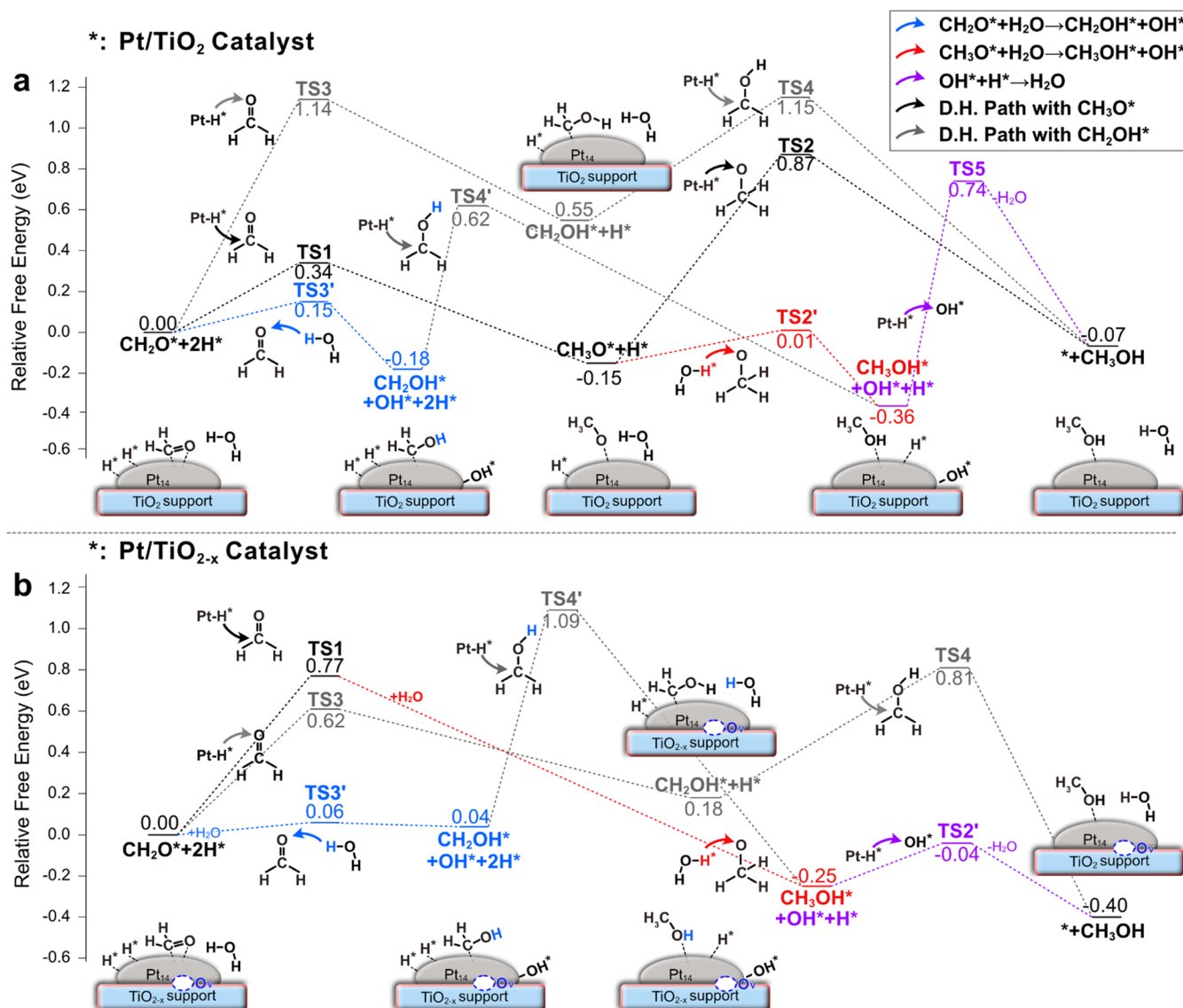

Figure 5. Relative free energies of the intermediates and transition states along with the aldehyde hydrogenation in aqueous phase. (a) On Pt/TiO_2. (b) On Pt/TiO_{2-x}. The proton participating the elementary step ($CH_2O^* + H_2O \rightarrow CH_2OH^* + OH^*$) is colored in blue, while the proton participating the elementary step ($CH_3O^* + H_2O \rightarrow CH_3OH^* + OH^*$) is colored in red, and the OH^* hydrogenation elementary step ($H^* + OH^* \rightarrow H_2O + 2^*$) is colored in purple. The corresponding 3D configurations are shown in Figure S9.

interface by proton transfer. This active $Pt-HO_{top}$ interaction will make the less polarized $Pt-O_{br}$ interface. However, with the presence of Ov, the Pt cluster will become negatively

charged, so its interaction with the HO_{top} might be suppressed. This again makes the polarization of the surface TiO_2 layer. Besides that, like the previous theoretical study on Au/TiO_2,[32]

we can also observe the more polarized charges of Pt atoms inside the cluster in aqueous phase than that in gas phase. The bottom of Pt_{14} cluster will be positively charged, while the higher part will be more negatively charged by water adsorption mentioned above.

In short, both the Ov on the support and the solvent water molecules could donate electrons to the Pt cluster in aqueous phase, within which the Ov plays the dominant role. After obtaining the equilibrium configurations of catalysts, we can further explore the catalytic mechanisms to illuminate the synergistic effect between Ov and solvent water molecules.

Aldehyde Hydrogenation in Aqueous Phase

As shown in Figure 3, the catalytic cycle of CH_2O hydrogenation typically includes the steps of reactant adsorption, hydrogenation, and product desorption. Among the various sites on the Pt cluster, previous studies[83,84] have confirmed that the low-coordinated sites are more favorable for adsorption. Therefore, the apical site exhibiting the lowest coordination number on top of the Pt cluster is used to adsorb CH_2O. Before the exploration in aqueous phase, we first conducted the formaldehyde (CH_2O) hydrogenation on both Pt/TiO_2 and Pt/TiO_{2-x} in gas phase as the reference. After the adsorption of CH_2O and H_2, the H* can first be added to either O or C, which can result in either the CH_2OH pathway (gray) or the CH_3O pathway (black), as shown in Figure 3a. Such hydrogenation of C and O atoms in aldehyde groups by the adsorbed H* directly is called the "direct hydrogenation mechanism" (D.H. mechanism) in the following discussion. As shown in Figure S7, on both Pt/TiO_2 and Pt/TiO_{2-x}, the CH_3O pathway is more favorable, and the Ov site does have a promotion effect in gas phase, which accords with the experiment.[27] Considering that the mechanism in gas phase is not the focal point of this work, the detailed discussion is shown in the Supporting Information.

Experiments have also shown the enhancement of aqueous phase on catalytic activity and selectivity in biomass hydrogenations.[21,30,42] Here, we employ the AIMD and MTD simulations to explore the mechanism of CH_2O hydrogenation within abundant explicit solvent water molecules. Due to the dynamic movement of solvent water molecules, it is hard to get the precise adsorption energies of CH_2O and H_2 by DFT in aqueous phase. Here, only the thermodynamics and kinetics of the elementary hydrogenation steps are accurately investigated. The reaction starts from the coadsorption state of CH_2O and H_2 ($CH_2O^* + 2H^*$), which is obtained from the AIMD simulation, followed by annealing and optimization.

During the AIMD simulations of $CH_2O^* + 2H^*$, one can observe the ambient hydrogen bonds (HBs) around the oxygen atom of CH_2O^*, which can be characterized by the radial distribution function (RDF) of HOH···O distances in Figure S8. When the hydrogenation proceeds, these solvent water molecules will not only form HBs with the intermediates, such as CH_3O^*, but also directly participate into the reaction cycle by proton transfers. These spontaneous proton transfers from solvent waters to CH_2O^* or CH_3O^* could occasionally take place in AIMD simulations. Hence, besides those direct hydrogenation (D.H.) steps, there are two extra elementary steps of proton transfer (P.T.) in aqueous phase, as shown in Figure 3b: (a) $CH_2O^* + H_2O + * \rightarrow CH_2OH^* + OH^*$ and (b) $CH_3O^* + H_2O + * \rightarrow CH_3OH^* + OH^*$. In the following calculation, we will get their free energy profiles by MTD simulations.

Essentially, these two P.T. steps are acid/base reactions at the solid/liquid interface. The O in the aldehyde group can be protonated by the adjacent solvent water and then via a Grotthuss-like mechanism[40,85,86] (vividly shown in Figure 4); the remaining OH^- in solution will simultaneously be transferred to adsorb on those comparatively more positive Pt atoms at the metal−support interface (see Figure 2b). These P.T. steps will not take place on the C in aldehyde group due to the repulsion between the proton and positively charged C, which is shown to be quite endergonic by around 1.0 eV with the high free barrier over 1.3 eV in Figure S10.

Now we can summarize the network of elementary reactions in aqueous phase. As shown in Figure 3b, the D.H. steps represent the direct H* addition to the C and O in the aldehyde group like the case in gas phase. The two brand-new P.T. steps involve the proton transfer from the solvent water to O of either CH_2O^* (blue arrow) or CH_3O^* (red arrow) to produce the OH^* at the metal−support interface. Then, the produced OH^* needs to undergo further hydrogenation (Hy.) to become the solvent water ($OH^* + H^* \rightarrow H_2O + 2^*$).

On Pt/TiO_2, the D.H. with the CH_2OH^* intermediate (gray lines in Figure 5a) calls for the free energy barrier of 1.15 eV (determined by $CH_2O^* + 2H$ and TS4), while the D.H. with the CH_3O^* intermediate (black lines in Figure 5a) exhibits the free energy barrier of 1.02 eV (determined by $CH_3O^* + H^*$ and TS2). Apparently, the direct hydrogenation with CH_3O^* is more favorable. Yet, in aqueous phase, the D.H. steps can be crossed with P.T. steps. Although the hydrogenation of C in the aldehyde group still follows the D.H. step, during the hydrogenation of its O, the P.T. steps are kinetically much easier than the D.H. steps. The proton in water can spontaneously transfer to CH_2O^* with the tiny G_a of 0.15 eV ($CH_2O^* + H_2O + * \rightarrow CH_2OH^* + OH^*$), which is exergonic by 0.18 eV. Similarly, the proton transfer to CH_3O^* is also exergonic by 0.21 eV with a small barrier of 0.16 eV ($CH_3O^* + H_2O + * \rightarrow CH_3OH^* + OH^*$). However, on Pt/TiO_2 without Ov, the generated OH^* suffers from the hard further hydrogenation with the relatively high G_a of 1.10 eV ($OH^* + H^* \rightarrow H_2O + 2^*$). This suggests that the OH^* could accumulate at the metal−support interface. The difficult OH^* hydrogenation could poison the Pt/TiO_2 catalyst, which suppresses the feasibility of those P.T. steps. By considering the whole reaction network, the D.H. step of C in CH_2O^*, followed by the facile P.T. step of CH_3O^* is the most favorable pathway on Pt/TiO_2. Due to its strong adsorption on the relative positive Pt atoms at the metal−support interface, the hydrogenation of the formed OH^* becomes the rate-determining step. According to the energetic span model[87] by Kozuch and Shaik, the turnover frequency (TOF)-determining intermediate (TDI) of the whole reaction is the $CH_3OH^* + OH^* + H^*$, and the TOF-determining transition state (TDTS) is the TS5. The overall free energy barrier ($G_{a,all}$) of the Pt/TiO_2 catalyst is 1.10 eV.

On Pt/TiO_{2-x}, the D.H. with the CH_2OH^* intermediate (gray lines in Figure 5b) calls for the free energy barrier of 0.81 eV (determined by $CH_2O^* + 2H^*$ and TS4). With the presence of Ov, the P.T. steps in Figure 5b will be more favorable over the reduced Pt cluster, and the CH_3O^* will no longer be a stable intermediate during the dynamic simulations. During MTD simulation of the D.H. step of C in CH_2O^* (black), the generated CH_3O^* will spontaneously convert to CH_3OH^* by proton transfer, generating the OH^* at the metal−support interface. Similarly, the CH_2O^* P.T. step

(blue) is also nearly barrierless in the free energy profile. More importantly, with Ov, the binding of OH* can be weakened by the more negative Pt cluster shown in Figure 1b. The hydrogenation of those generated OH* on Pt/TiO_{2-x} becomes not only exergonic by 0.15 eV but also kinetically much easier with G_a as low as 0.21 eV. By considering all of the possible steps, although the favorable pathway on Pt/TiO_{2-x} is the same with that on Pt/TiO_2, the TDI and TDTS have been altered due to the easier OH* hydrogenation. With the TDI of $CH_2O^* + 2H^*$ and TDTS of TS1, the $G_{a,all}$ on Pt/TiO_{2-x} is 0.77 eV (see Figure 5).

By exploring the reaction mechanisms of Pt/TiO_2 and Pt/TiO_{2-x} in aqueous phase, we can observe the synergistic effect between the oxygen vacancy and solvent water molecules. With the presence of the solvent water, there will be quite different mechanisms as shown in Figure 6. The C in the aldehyde
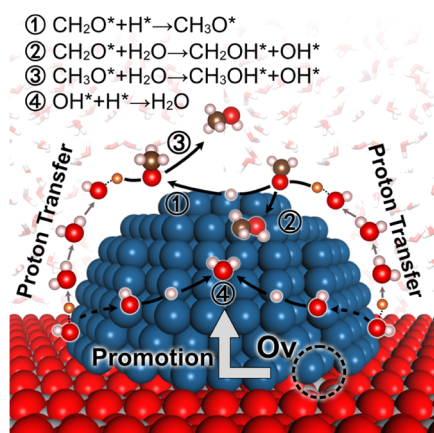

Figure 6. Schematic figure of formaldehyde hydrogenation including proton transfer steps and the detoxification of OH* on Pt/TiO_{2-x} in aqueous phase.

group will still be hydrogenated by direct H* addition, while the O in the aldehyde group will more favorably undergo the proton transfer mechanism, followed by the OH* hydrogenation. The proton can easily transfer from one adjacent solvent water to the O in the aldehyde group. Via a Grotthuss-

like mechanism in solvent water molecules, the remaining OH^- will simultaneously transfer to form the OH* at the metal–support interface. Such long-range proton transfer is important and common for heterogeneous catalysis in aqueous phase. Besides the promotion of solvent waters in experiments of biomass hydrogenation,[88,89] the isotopic studies confirmed the direct participation of water in hydrogenation through the proton transfer.[34] In addition, similar proton transfers were also observed at the Pt/CeO_2 interface in the previous AIMD simulations.[40]

However, without Ov, these negatively charged OH* would strongly adsorb on the positive Pt cluster and tend to poison the whole catalyst. The further hydrogenation of these OH* is endergonic by 0.29 eV on Pt/TiO_2 and suffers from the free energy barrier as high as 1.10 eV. This makes the accumulation of OH*, which could toxify the catalyst. A similar suppression effect coming from the strong base of potassium accumulated at the Pt/TiO_2 interfacial area is observed in the recent report of m-cresol hydrodeoxygenation.[90] Once the Pt is reduced by Ov, the binding of these OH* is weakened by the negatively charged Pt cluster. The OH* hydrogenation on Pt/TiO_{2-x} will become not only exergonic by 0.15 eV but also kinetically facile with the low barrier of 0.21 eV. Hence, as systematically shown in Figure 6, the synergistic promotion effect can be manifested by the proton transfer coming from solvent water molecules and the easier OH* hydrogenation coming from Ov.

After getting the free energy profiles of CH_2O hydrogenation in aqueous phase, we perform a roughly estimated microkinetic modeling (MKM) to give the vivid mechanistic insights. The details for this microkinetic model are provided in the Supporting Information. What should be noted is that with the established assumptions, the MKM result is in the scope of semiquantitative analyses rather than the accurate reaction rates. At the mild temperatures ranging from 273 to 373 K, when one compares the P.T. steps with D.H. steps (blue lines in Figure 7a), the fast P.T. steps on Pt/TiO_2 are largely suppressed by the lack of empty sites (*) due to the poisoning of OH*. When the Ov is presented, the OH* hydrogenation will be not only exergonic but also kinetically facile. Hence, the fast P.T. steps become the dominant processes on Pt/TiO_{2-x}. This makes the total reaction rate on Pt/TiO_{2-x} orders of magnitude faster than that on Pt/TiO_2
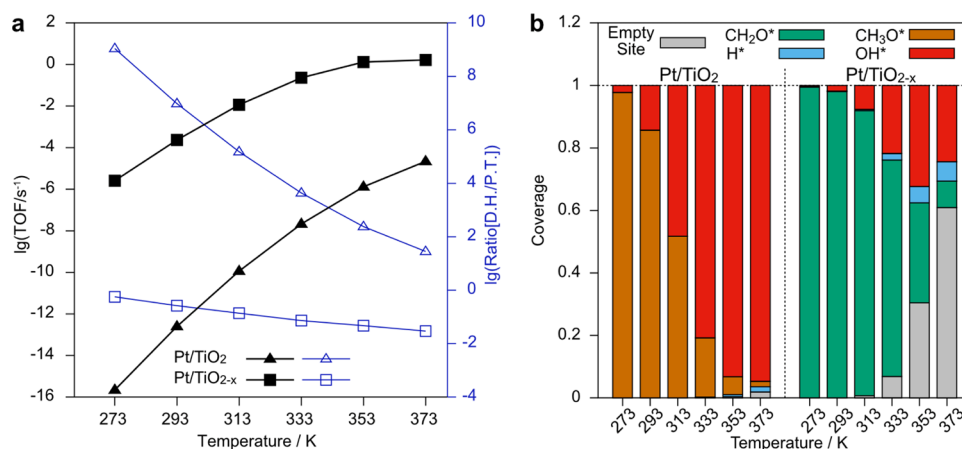

Figure 7. Steady-state kinetic results based on the roughly estimated microkinetic modeling in aqueous phase. (a) Total reaction TOF and the rate ratio (ratio[D.H./P.T.]) between the direct hydrogenation steps (D.H. of CH_2OH^* and CH_3O^*) and proton transfer steps (mainly determined by OH* hydrogenation). The detailed values are shown in Table S8. (b) Coverage of main species at the steady state under various reaction temperatures.

(black lines in Figure 7a). When the temperature is elevated to 373 K, the TOF on Pt/TiO$_{2-x}$ can reach the order of several s^{-1}. This result well accords with the obtained TOF ranging from 0.72 to 1.07 s^{-1} in the experiment of biomass hydrogenation at the mild conditions.[91] We can also observe this trend from the coverage consumed by OH* (θ_{OH*}) in Figure 7b under different reaction conditions. The Pt/TiO$_2$ is almost poisoned by OH*, and the empty sites ($\theta*$) can be as low as 10^{-2} even at the relative high temperature of 373 K. On Pt/TiO$_{2-x}$, θ_{OH*} decreases a lot and the $\theta*$ increases to around 0.61. This confirms that Ov can detoxicate the catalyst from the OH* accumulation, which can synergistically promote the aldehyde hydrogenation with solvent water molecules.

CONCLUSIONS

By AIMD simulations and DFT calculations, the aldehyde hydrogenation on the Pt/TiO$_2$ catalysts in aqueous phase is explored theoretically within the more realistic ternary model involving all of the metal, the oxide support, and the explicit solvent water molecules. By comparing the catalytic mechanisms over the Pt/TiO$_2$ and Pt/TiO$_{2-x}$ catalysts, the synergistic promotion effect between the oxygen vacancy (Ov) and solvent water molecules is observed. (I) In aqueous phase, both the Ov on support and the solvent water molecules could donate electrons to the Pt cluster. The Ov plays a dominant role and can reduce the Pt cluster from positive to negative. (II) In aqueous phase, the solvent water molecules could spontaneously protonate O in the aldehyde group by acid/base exchange, generating the OH* at the metal−support interface by long-range proton transfer. Although the C in the aldehyde group still follows the direct hydrogenation mechanism, such water-mediated proton transfer is more facile for adding H to O in the aldehyde group. (III) The OH* can bind strongly on the positively charged Pt cluster over stoichiometric TiO$_2$, hindering its further hydrogenation. This could poison the catalyst and suppress the promotion of proton transfer steps, while on the reduced Pt cluster over TiO$_{2-x}$ with Ov, the OH* hydrogenation becomes not only exergonic but also kinetically more facile. The Ov can protect the catalyst from poisoning and synergistically help the proton transfer steps, which synergistically promote aldehyde hydrogenation with solvent waters. To the broad chemist community, this work shows the importance of realistic modeling. The catalytic reaction in aqueous phase is not only related to the surface of the metal cluster or nanoparticle. Even for such a simple hydrogenation (CH$_2$O + H$_2$ → CH$_3$OH), the mechanism is related to all of the metal, oxide support, and solvent waters. Considering the ubiquity of Ov on reducible oxide supports and the commonly used aqueous catalytic conditions, this synergistic effect between the oxygen vacancy and solvent water molecules may not be limited to the Pt/TiO$_{2-x}$ catalyst, which can shed light on the rational design of supported metal catalysts for biomass conversion and upgrading.

ASSOCIATED CONTENT

Supporting Information

The Supporting Information is available free of charge at https://pubs.acs.org/doi/10.1021/jacsau.2c00560.

Details on the theoretical models and AIMD simulations, detailed parameters and tests on MTD simulations, energy profiles, radius distribution function,

microkinetic modeling results, and details on charge analysis (PDF)

AUTHOR INFORMATION

Corresponding Authors

Guang-Jie Xia − *Department of Chemistry and Guangdong Provincial Key Laboratory of Catalysis, Southern University of Science and Technology, Shenzhen 518055 Guangdong, China;* orcid.org/0000-0002-4892-6289; Email: xiagj@sustech.edu.cn

Yang-Gang Wang − *Department of Chemistry and Guangdong Provincial Key Laboratory of Catalysis, Southern University of Science and Technology, Shenzhen 518055 Guangdong, China;* orcid.org/0000-0002-0582-0855; Email: wangyg@sustech.edu.cn

Authors

Wei Cao − *Department of Chemistry and Guangdong Provincial Key Laboratory of Catalysis, Southern University of Science and Technology, Shenzhen 518055 Guangdong, China*

Zhen Yao − *Department of Chemistry and Guangdong Provincial Key Laboratory of Catalysis, Southern University of Science and Technology, Shenzhen 518055 Guangdong, China;* orcid.org/0000-0002-3782-1027

Ke-Han Zeng − *Department of Chemistry and Guangdong Provincial Key Laboratory of Catalysis, Southern University of Science and Technology, Shenzhen 518055 Guangdong, China*

Ying Qiao − *Department of Chemistry and Guangdong Provincial Key Laboratory of Catalysis, Southern University of Science and Technology, Shenzhen 518055 Guangdong, China*

Complete contact information is available at:
https://pubs.acs.org/10.1021/jacsau.2c00560

Notes

The authors declare no competing financial interest.

REFERENCES

(1) Tuck, C. O.; Pérez, E.; Horváth, I. T.; Sheldon, R. A.; Poliakoff, M. Valorization of Biomass: Deriving More Value from Waste. *Science* **2012**, *337*, 695−699.

(2) Serrano-Ruiz, J. C.; West, R. M.; Dumesic, J. A. Catalytic Conversion of Renewable Biomass Resources to Fuels and Chemicals. *Annu. Rev. Chem. Biomol. Eng.* **2010**, *1*, 79−100.

(3) Mullen, C. A.; Strahan, G. D.; Boateng, A. A. Characterization of Various Fast-Pyrolysis Bio-Oils by NMR Spectroscopy. *Energy Fuels* **2009**, *23*, 2707−2718.

(4) Hao, N.; Ben, H.; Yoo, C. G.; Adhikari, S.; Ragauskas, A. J. Review of NMR Characterization of Pyrolysis Oils. *Energy Fuels* **2016**, *30*, 6863−6880.

(5) Negahdar, L.; Gonzalez-Quiroga, A.; Otyuskaya, D.; Toraman, H. E.; Liu, L.; Jastrzebski, J. T. B. H.; Van Geem, K. M.; Marin, G. B.; Thybaut, J. W.; Weckhuysen, B. M. Characterization and Comparison of Fast Pyrolysis Bio-Oils from Pinewood, Rapeseed Cake, and Wheat Straw Using 13C NMR and Comprehensive GC × GC. *ACS Sustainable Chem. Eng.* **2016**, *4*, 4974−4985.

(6) Guisnet, M.; Magnoux, P. Organic Chemistry of Coke Formation. *Appl. Catal., A* **2001**, *212*, 83−96.

(7) Cantu, D. C.; Padmaperuma, A. B.; Nguyen, M. T.; Akhade, S. A.; Yoon, Y.; Wang, Y. G.; Lee, M. S.; Glezakou, V. A.; Rousseau, R.; Lilga, M. A. A Combined Experimental and Theoretical Study on the Activity and Selectivity of the Electrocatalytic Hydrogenation of Aldehydes. *ACS Catal.* **2018**, *8*, 7645−7658.

(8) Mortensen, P. M.; Grunwaldt, J. D.; Jensen, P. A.; Knudsen, K. G.; Jensen, A. D. A Review of Catalytic Upgrading of Bio-Oil to Engine Fuels. *Appl. Catal., A* **2011**, *407*, 1−19.

(9) Wang, H.; Male, J.; Wang, Y. Recent Advances in Hydrotreating of Pyrolysis Bio-Oil and Its Oxygen-Containing Model Compounds. *ACS Catal.* **2013**, *3*, 1047−1070.

(10) Elliott, D. C. Historical Developments in Hydroprocessing Bio-Oils. *Energy Fuels* **2007**, *21*, 1792−1815.

(11) Al-Sabawi, M.; Chen, J.; Ng, S. Fluid Catalytic Cracking of Biomass-Derived Oils and Their Blends with Petroleum Feedstocks: A Review. *Energy Fuels* **2012**, *26*, 5355−5372.

(12) Salaeh, R.; Faungnawakij, K.; Kungwan, N.; Hirunsit, P. The Role of Metal Species on Aldehyde Hydrogenation over Co13 and Ni13 Supported on γ-Al2O3(110) Surfaces: A Theoretical Study. *ChemistrySelect* **2020**, *5*, 4058−4068.

(13) Procházková, D.; Zámostný, P.; Bejblová, M.; Červený, L.; Čejka, J. Hydrodeoxygenation of Aldehydes Catalyzed by Supported Palladium Catalysts. *Appl. Catal., A* **2007**, *332*, 56−64.

(14) Li, X.; Jia, P.; Wang, T. Furfural: A Promising Platform Compound for Sustainable Production of C4 and C5 Chemicals. *ACS Catal.* **2016**, *6*, 7621−7640.

(15) Pei, Y.; Wang, J.; Fu, Q.; Guo, P.; Qiao, M.; Yan, S.; Fan, K. A Non-Noble Amorphous Co-Fe-B Catalyst Highly Selective in Liquid Phase Hydrogenation of Crotonaldehyde to Crotyl Alcohol. *New J. Chem.* **2005**, *29*, 992−994.

(16) Gates, B. C. Supported Metal Clusters: Synthesis, Structure, and Catalysis. *Chem. Rev.* **1995**, *95*, 511−522.

(17) Dong, C.; Li, Y.; Cheng, D.; Zhang, M.; Liu, J.; Wang, Y.-G.; Xiao, D.; Ma, D. Supported Metal Clusters: Fabrication and Application in Heterogeneous Catalysis. *ACS Catal.* **2020**, *10*, 11011−11045.

(18) Mäki-Arvela, P.; Hájek, J.; Salmi, T.; Murzin, D. Y. Chemoselective Hydrogenation of Carbonyl Compounds over Heterogeneous Catalysts. *Appl. Catal., A* **2005**, *292*, 1−49.

(19) Kennedy, G.; Baker, L. R.; Somorjai, G. A. Selective Amplification of C=O Bond Hydrogenation on Pt/TiO2: Catalytic Reaction and Sum-Frequency Generation Vibrational Spectroscopy Studies of Crotonaldehyde Hydrogenation. *Angew. Chem., Int. Ed.* **2014**, *53*, 3405−3408.

(20) Albilali, R.; Douthwaite, M.; He, Q.; Taylor, S. H. The Selective Hydrogenation of Furfural over Supported Palladium Nanoparticle Catalysts Prepared by Sol-Immobilisation: Effect of Catalyst Support and Reaction Conditions. *Catal. Sci. Technol.* **2018**, *8*, 252−267.

(21) Ramos, R.; Tišler, Z.; Kikhtyanin, O.; Kubička, D. Solvent Effects in Hydrodeoxygenation of Furfural-Acetone Aldol Condensation Products over Pt/TiO2 Catalyst. *Appl. Catal., A* **2017**, *530*, 174−183.

(22) Xia, G.-J.; Lee, M.-S.; Glezakou, V.-A.; Rousseau, R.; Wang, Y.-G. Diffusion and Surface Segregation of Interstitial Ti Defects Induced by Electronic Metal−Support Interactions on a Au/TiO2 Nanocatalyst. *ACS Catal.* **2022**, *12*, 4455−4464.

(23) Saqlain, M. A.; Hussain, A.; Siddiq, M.; Ferreira, A. R.; Leitão, A. A. Thermally Activated Surface Oxygen Defects at the Perimeter of Au/TiO2: A DFT+U Study. *Phys. Chem. Chem. Phys.* **2015**, *17*, 25403−25410.

(24) Wang, Y.-G.; Yoon, Y.; Glezakou, V.-A.; Li, J.; Rousseau, R. The Role of Reducible Oxide-Metal Cluster Charge Transfer in Catalytic Processes: New Insights on the Catalytic Mechanism of CO Oxidation on Au/TiO2 from Ab Initio Molecular Dynamics. *J. Am. Chem. Soc.* **2013**, *135*, 10673−10683.

(25) Wang, Y. G.; Cantu, D. C.; Lee, M. S.; Li, J.; Glezakou, V. A.; Rousseau, R. CO Oxidation on Au/TiO2: Condition-Dependent Active Sites and Mechanistic Pathways. *J. Am. Chem. Soc.* **2016**, *138*, 10467−10476.

(26) Kalamaras, C. M.; Panagiotopoulou, P.; Kondarides, D. I.; Efstathiou, A. M. Kinetic and Mechanistic Studies of the Water-Gas Shift Reaction on Pt/TiO2 Catalyst. *J. Catal.* **2009**, *264*, 117−129.

(27) Li, J.; Zhou, H.; Zhuo, H.; Wei, Z.; Zhuang, G.; Zhong, X.; Deng, S.; Li, X.; Wang, J. Oxygen Vacancies on TiO2 Promoted the Activity and Stability of Supported Pd Nanoparticles for the Oxygen Reduction Reaction. *J. Mater. Chem. A* **2018**, *6*, 2264−2272.

(28) Qiu, H.; Ma, X.; Sun, C.; Zhao, B.; Chen, F. Surface Oxygen Vacancies Enriched Pt/TiO2 Synthesized with a Defect Migration Strategy for Superior Photocatalytic Activity. *Appl. Surf. Sci.* **2020**, *506*, No. 145021.

(29) Ammal, S. C.; Heyden, A. Modeling the Noble Metal/TiO2 (110) Interface with Hybrid DFT Functionals: A Periodic Electrostatic Embedded Cluster Model Study. *J. Chem. Phys.* **2010**, *133*, No. 164703.

(30) Lee, C. B. T. L.; Wu, T. Y. A Review on Solvent Systems for Furfural Production from Lignocellulosic Biomass. *Renewable Sustainable Energy Rev.* **2021**, *137*, No. 110172.

(31) Gallezot, P. Conversion of Biomass to Selected Chemical Products. *Chem. Soc. Rev.* **2012**, *41*, 1538−1558.

(32) Camellone, M. F.; Marx, D. On the Impact of Solvation on a Au/TiO2 Nanocatalyst in Contact with Water. *J. Phys. Chem. Lett.* **2013**, *4*, 514−518.

(33) Li, K.; Deng, L.; Yi, S.; Wu, Y.; Xia, G.; Zhao, J.; LU, D.; Min, Y. Boosting the Performance by the Water Solvation Shell with Hydrogen Bonds on Protonic Ionic Liquids: Insights into the Acid Catalysis of the Glycosidic Bond. *Catal. Sci. Technol.* **2021**, *11*, 3527−3538.

(34) Shangguan, J.; Chin, Y. H. C. Kinetic Significance of Proton-Electron Transfer during Condensed Phase Reduction of Carbonyls on Transition Metal Clusters. *ACS Catal.* **2019**, *9*, 1763−1778.

(35) Zhao, Z.; Bababrik, R.; Xue, W.; Li, Y.; Briggs, N. M.; Nguyen, D. T.; Nguyen, U.; Crossley, S. P.; Wang, S.; Wang, B.; Resasco, D. E. Solvent-Mediated Charge Separation Drives Alternative Hydrogenation Path of Furanics in Liquid Water. *Nat. Catal.* **2019**, *2*, 431−436.

(36) Cao, H.; Xia, G. J.; Chen, J. W.; Yan, H. M.; Huang, Z.; Wang, Y. G. Mechanistic Insight into the Oxygen Reduction Reaction on the Mn-N4/C Single-Atom Catalyst: The Role of the Solvent Environment. *J. Phys. Chem. C* **2020**, *124*, 7287−7294.

(37) Liu, Y.; Baráth, E.; Shi, H.; Hu, J.; Camaioni, D. M.; Lercher, J. A. Solvent-Determined Mechanistic Pathways in Zeolite-H-BEA-Catalysed Phenol Alkylation. *Nat. Catal.* **2018**, *1*, 141−147.

(38) Andanson, J. M.; Baiker, A. Exploring Catalytic Solid/Liquid Interfaces by in Situ Attenuated Total Reflection Infrared Spectroscopy. *Chem. Soc. Rev.* **2010**, *39*, 4571−4584.

(39) Meier, D. M.; Urakawa, A.; Baiker, A. In Situ PM-IRRAS Study of Liquid-Phase Benzyl Alcohol Oxidation on Palladium. *J. Phys. Chem. C* **2009**, *113*, 21849−21855.

(40) Farnesi Camellone, M.; Negreiros Ribeiro, F.; Szabová, L.; Tateyama, Y.; Fabris, S. Catalytic Proton Dynamics at the Water/Solid Interface of Ceria-Supported Pt Clusters. *J. Am. Chem. Soc.* **2016**, *138*, 11560−11567.

(41) Cheng, J.; Sprik, M. Acidity of the Aqueous Rutile TiO2 (110) Surface from Density Functional Theory Based Molecular Dynamics. *J. Chem. Theory Comput.* **2010**, *6*, 880−889.

(42) Li, G.; Wang, B.; Resasco, D. E. Water-Mediated Heterogeneously Catalyzed Reactions. *ACS Catal.* **2020**, *10*, 1294−1309.

(43) Shangguan, J.; Olarte, M. V.; Chin, Y. H. Mechanistic Insights on C-O and C-C Bond Activation and Hydrogen Insertion during Acetic Acid Hydrogenation Catalyzed by Ruthenium Clusters in Aqueous Medium. *J. Catal.* **2016**, *340*, 107−121.

(44) Migliore, A.; Polizzi, N. F.; Therien, M. J.; Beratan, D. N. Biochemistry and Theory of Proton-Coupled Electron Transfer. *Chem. Rev.* **2014**, *114*, 3381−3465.

(45) Mulkidjanian, A. Y.; Cherepanov, D. A.; Heberle, J.; Junge, W. Proton Transfer Dynamics at Membrane/Water Interface and Mechanism of Biological Energy Conversion. *Biochemistry* **2005**, *70*, 251−256.

(46) Yuk, S. F.; Lee, M. S.; Akhade, S. A.; Nguyen, M. T.; Glezakou, V. A.; Rousseau, R. First-Principle Investigation on Catalytic Hydrogenation of Benzaldehyde over Pt-Group Metals. *Catal. Today* **2022**, *388−389*, 208−215.

(47) Wang, J.; Lv, C. Q.; Liu, J. H.; Ren, R. R.; Wang, G. C. Theoretical Investigation of Solvent Effects on the Selective Hydrogenation of Furfural over Pt(111). *Int. J. Hydrogen Energy* **2021**, *46*, 1592−1604.

(48) Liu, J. C.; Tang, Y.; Chang, C. R.; Wang, Y. G.; Li, J. Mechanistic Insights into Propene Epoxidation with O2-H2O Mixture on Au7/α-Al2O3: A Hydroproxyl Pathway from Ab Initio Molecular Dynamics Simulations. *ACS Catal.* **2016**, *6*, 2525−2535.

(49) Xia, G.-J.; Wang, Y.-G. Solvent Promotion on the Metal-Support Interaction and Activity of Pd@ZrO2 Catalyst: Formation of Metal Hydrides as the New Catalytic Active Phase at the Solid-Liquid Interface. *J. Catal.* **2021**, *404*, 537−550.

(50) Vandevondele, J.; Krack, M.; Mohamed, F.; Parrinello, M.; Chassaing, T.; Hutter, J. Quickstep: Fast and Accurate Density Functional Calculations Using a Mixed Gaussian and Plane Waves Approach. *Comput. Phys. Commun.* **2005**, *167*, 103−128.

(51) Perdew, J. P.; Burke, K.; Ernzerhof, M. Generalized Gradient Approximation Made Simple. *Phys. Rev. Lett.* **1996**, *77*, 3865−3868.

(52) Grimme, S.; Antony, J.; Ehrlich, S.; Krieg, H. A Consistent and Accurate Ab Initio Parametrization of Density Functional Dispersion Correction (DFT-D) for the 94 Elements H-Pu. *J. Chem. Phys.* **2010**, *132*, No. 154104.

(53) Arroyo-De Dompablo, M. E.; Morales-Garca, A.; Taravillo, M. DFTU Calculations of Crystal Lattice, Electronic Structure, and Phase Stability under Pressure of TiO2 Polymorphs. *J. Chem. Phys.* **2011**, *135*, No. 054503.

(54) Kowalski, P. M.; Camellone, M. F.; Nair, N. N.; Meyer, B.; Marx, D. Charge Localization Dynamics Induced by Oxygen Vacancies on the TiO 2(110) Surface. *Phys. Rev. Lett.* **2010**, *105*, No. 146405.

(55) Rodríguez-Fortea, A.; Iannuzzi, M. First-Principles Molecular Dynamics Study of the Heterogeneous Reduction of NO2 on Soot Surfaces. *J. Phys. Chem. C* **2008**, *112*, 19642−19648.

(56) Barducci, A.; Bonomi, M.; Parrinello, M. Metadynamics. *Wiley Interdiscip. Rev. Comput. Mol. Sci.* **2011**, *1*, 826−843.

(57) Evans, D. J.; Holian, B. L. The Nose−Hoover Thermostat. *J. Chem. Phys.* **1985**, *83*, No. 4069.

(58) Newman, C.; Zhou, X.; Goundie, B.; Ghampson, I. T.; Pollock, R. A.; Ross, Z.; Wheeler, M. C.; Meulenberg, R. W.; Austin, R. N.; Frederick, B. G. Effects of Support Identity and Metal Dispersion in Supported Ruthenium Hydrodeoxygenation Catalysts. *Appl. Catal., A* **2014**, *477*, 64−74.

(59) Macino, M.; Barnes, A. J.; Althahban, S. M.; Qu, R.; Gibson, E. K.; Morgan, D. J.; Freakley, S. J.; Dimitratos, N.; Kiely, C. J.; Gao, X.; Beale, A. M.; Bethell, D.; He, Q.; Sankar, M.; Hutchings, G. J. Tuning of Catalytic Sites in Pt/TiO2 Catalysts for the Chemoselective Hydrogenation of 3-Nitrostyrene. *Nat. Catal.* **2019**, *2*, 873−881.

(60) Zhou, Y.; King, D. M.; Liang, X.; Li, J.; Weimer, A. W. Optimal Preparation of Pt/TiO2 Photocatalysts Using Atomic Layer Deposition. *Appl. Catal., B* **2010**, *101*, 54−60.

(61) Hartke, B.; Carter, E. A. Ab Initio Molecular Dynamics with Correlated Molecular Wave Functions: Generalized Valence Bond Molecular Dynamics and Simulated Annealing. *J. Chem. Phys.* **1992**, *97*, 6569−6578.

(62) Hartke, B.; Carter, E. A. Ab Initio Molecular Dynamics Simulated Annealing at the Generalized Valence Bond Level. Application to a Small Nickel Cluster. *Chem. Phys. Lett.* **1993**, *216*, 324−328.

(63) Laio, A.; Gervasio, F. L. Metadynamics: A Method to Simulate Rare Events and Reconstruct the Free Energy in Biophysics, Chemistry and Material Science. *Rep. Prog. Phys.* **2008**, *71*, No. 126601.

(64) Gervasio, F. L.; Laio, A.; Parrinello, M. Flexible Docking in Solution Using Metadynamics. *J. Am. Chem. Soc.* **2005**, *127*, 2600−2607.

(65) Bucko, T. Ab Initio Calculations of Free-Energy Reaction Barriers. *J. Phys.: Condens. Matter* **2008**, *20*, No. 064211.

(66) Kuo, C.-T.; Lu, Y.; Kovarik, L.; Engelhard, M.; Karim, A. M. Structure Sensitivity of Acetylene Semi-Hydrogenation on Pt Single Atoms and Subnanometer Clusters. *ACS Catal.* **2019**, *9*, 11030−11041.

(67) Wang, W. N.; An, W. J.; Ramalingam, B.; Mukherjee, S.; Niedzwiedzki, D. M.; Gangopadhyay, S.; Biswas, P. Size and Structure Matter: Enhanced CO 2 Photoreduction Efficiency by Size-Resolved Ultrafine Pt Nanoparticles on TiO 2 Single Crystals. *J. Am. Chem. Soc.* **2012**, *134*, 11276−11281.

(68) Dessal, C.; Martínez, L.; Maheu, C.; Len, T.; Morfin, F.; Rousset, J. L.; Puzenat, E.; Afanasiev, P.; Aouine, M.; Soler, L.; Llorca, J.; Piccolo, L. Influence of Pt Particle Size and Reaction Phase on the Photocatalytic Performances of Ultradispersed Pt/TiO2 Catalysts for Hydrogen Evolution. *J. Catal.* **2019**, *375*, 155−163.

(69) Vajda, S.; Pellin, M. J.; Greeley, J. P.; Marshall, C. L.; Curtiss, L. A.; Ballentine, G. A.; Elam, J. W.; Catillon-Mucherie, S.; Redfern, P. C.; Mehmood, F.; Zapol, P. Subnanometre Platinum Clusters as Highly Active and Selective Catalysts for the Oxidative Dehydrogenation of Propane. *Nat. Mater.* **2009**, *8*, 213−216.

(70) Bi, X.; Du, G.; Kalam, A.; Sun, D.; Yu, Y.; Su, Q.; Xu, B.; Al-Sehemi, A. G. Tuning Oxygen Vacancy Content in TiO2 Nanoparticles to Enhance the Photocatalytic Performance. *Chem. Eng. Sci.* **2021**, *234*, No. 116440.

(71) Sanchez, M. G.; Gazquez, J. L. Oxygen Vacancy Model in Strong Metal-Support Interaction. *J. Catal.* **1987**, *104*, 120−135.

(72) Liu, Y.; Miao, C.; Yang, P.; He, Y.; Feng, J.; Li, D. Synergetic Promotional Effect of Oxygen Vacancy-Rich Ultrathin TiO2 and Photochemical Induced Highly Dispersed Pt for Photoreduction of CO2 with H2O. *Appl. Catal., B* **2019**, *244*, 919−930.

(73) Pan, X.; Yang, M. Q.; Fu, X.; Zhang, N.; Xu, Y. J. Defective TiO2 with Oxygen Vacancies: Synthesis, Properties and Photocatalytic Applications. *Nanoscale* **2013**, *5*, 3601−3614.

(74) Ren, Z.; Liu, N.; Chen, B.; Li, J.; Mei, D. Theoretical Investigation of the Structural Stabilities of Ceria Surfaces and Supported Metal Nanocluster in Vapor and Aqueous Phases. *J. Phys. Chem. C* **2018**, *122*, 4828−4840.

(75) Fu, Q.; Wagner, T.; Olliges, S.; Carstanjen, H. D. Metal-Oxide Interfacial Reactions: Encapsulation of Pd on TiO2 (110). *J. Phys. Chem. B* **2005**, *109*, 944−951.

(76) Geng, Z.; Jin, X.; Wang, R.; Chen, X.; Guo, Q.; Ma, Z.; Dai, D.; Fan, H.; Yang, X. Low-Temperature Hydrogen Production via Water Conversion on Pt/TiO2. *J. Phys. Chem. C* **2018**, *122*, 10956−10962.

(77) Oyekan, K. A.; Van de Put, M.; Tiwari, S.; Rossi, C.; Esteve, A.; Vandenberghe, W. Re-Examining the Role of Subsurface Oxygen Vacancies in the Dissociation of H2O Molecules on Anatase TiO2. *Appl. Surf. Sci.* **2022**, *594*, No. 153452.

(78) Henkelman, G.; Arnaldsson, A.; Jónsson, H. A Fast and Robust Algorithm for Bader Decomposition of Charge Density. *Comput. Mater. Sci.* **2006**, *36*, 354−360.

(79) Tang, W.; Sanville, E.; Henkelman, G. A Grid-Based Bader Analysis Algorithm without Lattice Bias. *J. Phys.: Condens. Matter* **2009**, *21*, No. 084204.

(80) Zhang, S.; Xia, Z.; Ni, T.; Zhang, Z.; Ma, Y.; Qu, Y. Strong Electronic Metal-Support Interaction of Pt/CeO2 Enables Efficient and Selective Hydrogenation of Quinolines at Room Temperature. *J. Catal.* **2018**, *359*, 101−111.

(81) Wang, Y. G.; Yoon, Y.; Glezakou, V. A.; Li, J.; Rousseau, R. The Role of Reducible Oxide-Metal Cluster Charge Transfer in Catalytic Processes: New Insights on the Catalytic Mechanism of CO Oxidation on Au/TiO2 from Ab Initio Molecular Dynamics. *J. Am. Chem. Soc.* **2013**, *135*, 10673−10683.

(82) Aso, R.; Hojo, H.; Takahashi, Y.; Akashi, T.; Midoh, Y.; Ichihashi, F.; Nakajima, H.; Tamaoka, T.; Yubuta, K.; Nakanishi, H.; Einaga, H.; Tanigaki, T.; Shinada, H.; Murakami, Y. Direct Identification of the Charge State in a Single Platinum Nanoparticle on Titanium Oxide. *Science* **2022**, *378*, 202−206.

(83) Lopez, N.; Janssens, T. V. W.; Clausen, B. S.; Xu, Y.; Mavrikakis, M.; Bligaard, T.; Nørskov, J. K. On the Origin of the Catalytic Activity of Gold Nanoparticles for Low-Temperature CO Oxidation. *J. Catal.* **2004**, *223*, 232−235.

(84) Calle-Vallejo, F.; Loffreda, D.; Koper, M. T. M.; Sautet, P. Introducing Structural Sensitivity into Adsorption-Energy Scaling Relations by Means of Coordination Numbers. *Nat. Chem.* **2015**, *7*, 403−410.

(85) Cukierman, S. Et Tu, Grotthuss! And Other Unfinished Stories. *Biochim. Biophys. Acta* **2006**, *1757*, 876−885.

(86) Merte, L. R.; Peng, G.; Bechstein, R.; Rieboldt, F.; Farberow, C. A.; Grabow, L. C.; Kudernatsch, W.; Wendt, S.; Lægsgaard, E.; Mavrikakis, M.; Besenbacher, F. Water-Mediated Proton Hopping on an Iron Oxide Surface. *Science* **2012**, *336*, 889−893.

(87) Kozuch, S.; Shaik, S. How to Conceptualize Catalytic Cycles? The Energetic Span Model. *Acc. Chem. Res.* **2011**, *44*, 101−110.

(88) Seretis, A.; Diamantopoulou, P.; Thanou, I.; Tzevelekidis, P.; Fakas, C.; Lilas, P.; Papadogianakis, G. Recent Advances in Ruthenium-Catalyzed Hydrogenation Reactions of Renewable Bio-mass-Derived Levulinic Acid in Aqueous Media. *Front. Chem.* **2020**, *8*, 221.

(89) Papadogianakis, G.; Sheldon, R. A.; Murzin, D. Y.; Wu, Y. Editorial: Aqueous-Phase Catalytic Conversions of Renewable Feedstocks for Sustainable Biorefineries. *Front. Chem.* **2020**, *8*, 629578.

(90) Lin, F.; Lu, Y.; Unocic, K. A.; Habas, S. E.; Griffin, M. B.; Schaidle, J. A.; Meyer, H. M.; Wang, Y.; Wang, H. Deactivation by Potassium Accumulation on a Pt/TiO2 Bifunctional Catalyst for Biomass Catalytic Fast Pyrolysis. *ACS Catal.* **2022**, *12*, 465−480.

(91) Cattaneo, S.; Capelli, S.; Stucchi, M.; Bossola, F.; Dal Santo, V.; Araujo-Lopez, E.; Sharapa, D. I.; Studt, F.; Villa, A.; Chieregato, A.; Vandegehuchte, B. D.; Prati, L. Discovering the Role of Substrate in Aldehyde Hydrogenation. *J. Catal.* **2021**, *399*, 162−169.